

Prompt-Based Test-Time Real Image Dehazing: A Novel Pipeline

Zixuan Chen, Zewei He*, Ziqian Lu, Xuecheng Sun, Zhe-Ming Lu
Zhejiang University, Hangzhou, China

{22224039, zeweihe, ziqianlu, xuechengsun, zheminglu}@zju.edu.cn

Abstract

Existing methods attempt to improve models' generalization ability on real-world hazy images by exploring well-designed training schemes (e.g., CycleGAN, prior loss). However, most of them need very complicated training procedures to achieve satisfactory results. In this work, we present a totally novel testing pipeline called Prompt-based Test-Time Dehazing (PTTD) to help generate visually pleasing results of real-captured hazy images during the inference phase. We experimentally find that given a dehazing model trained on synthetic data, by fine-tuning the statistics (i.e., mean and standard deviation) of encoding features, PTTD is able to narrow the domain gap, boosting the performance of real image dehazing. Accordingly, we first apply a prompt generation module (PGM) to generate a visual prompt, which is the source of appropriate statistical perturbations for mean and standard deviation. And then, we employ the feature adaptation module (FAM) into the existing dehazing models for adjusting the original statistics with the guidance of the generated prompt. Note that, PTTD is model-agnostic and can be equipped with various state-of-the-art dehazing models trained on synthetic hazy-clean pairs. Extensive experimental results demonstrate that our PTTD is flexible meanwhile achieves superior performance against state-of-the-art dehazing methods in real-world scenarios. The code will be released at <https://github.com/cecret3350/PTTD-Dehazing>.

1. Introduction

Hazy images often suffer from low contrast, poor visibility, and color distortion [44], imposing a negative impact on the downstream high-level vision tasks, such as object detection, image classification, and semantic segmentation. According to the atmospheric scattering model (ASM) [36, 37], the hazing process is commonly formulated as:

$$I(x) = J(x)t(x) + A(1 - t(x)), \quad (1)$$

*Corresponding author.

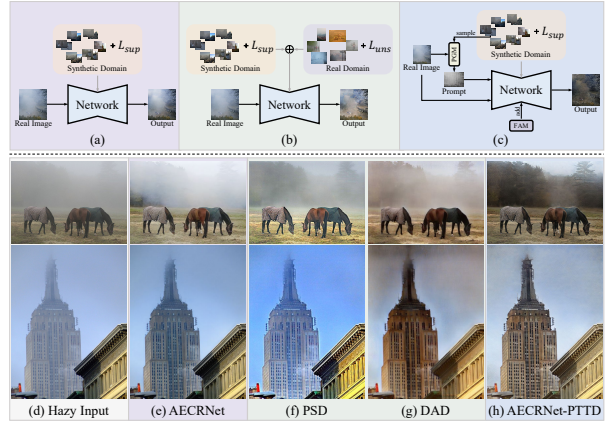


Figure 1. Different frameworks and their results on real-world hazy images. (a) Directly apply model trained on synthetic data to real hazy image; (b) Use synthetic and real data together to train the model and then apply it to real hazy image; (c) Our proposed PTTD utilizes the model pre-trained on synthetic data and modifies the extracted features in the inference phase; (d) Real hazy images; and (e-h) Processing results of AECRNet [45], PSD [10], DAD [41] and our proposed PTTD (by adopting pre-trained AE-CRNet [45]). It is worth mentioning that AE-CR-PTTD achieves very promising results.

where $I(x)$ is the observed hazy image and $J(x)$ denotes the clean image of the same scene. A and $t(x)$ are the global atmospheric light and the transmission map, respectively.

Image dehazing aims to recover the haze-free image from corresponding hazy input, which is a highly ill-posed problem. Early approaches tend to solve this challenge by introducing various priors, such as Dark Channel Prior (DCP) [20, 21], Non-Local Prior (NLP) [6], Color Attenuation Prior (CAP) [53], etc. However, real-world hazy images do not always satisfy the priors and artifacts may be introduced under this condition.

With the rising of deep learning, researchers have proposed a series of single image dehazing methods based on convolutional neural networks (CNNs). Most of them try to estimate the $t(x)$ and A [8, 28, 40] in Eq. (1) or directly learn the latent haze-free image (or haze residual)

[13, 23, 38, 45, 52]. The former then utilizes the estimated $t(x)$ and A to derive the haze-free image via ASM.

Recently, existing deep learning based dehazing methods are devoted to improving performance by training sophisticated architectures on synthetic datasets [11, 52]. Though breakthrough progress has been made in the past decade, the processing results on real-captured hazy images are still unsatisfactory (as shown in Fig. 1 (e)), and it is mainly caused by the domain shift. How to bridge the gap between synthetic and real-world data is a hot research topic among the computer vision community.

In order to improve the models’ generalization ability on real-world hazy images, researchers start exploring CycleGAN based [41, 47] and prior loss based [10, 18] methods. However, either CycleGAN based or prior loss based methods demand very complex training procedures to guarantee the performance. Moreover, the former tends to produce results with artifacts (Fig. 1 (g)), whereas the latter is negatively influenced by the inherent deficiencies of physical priors (Fig. 1 (f)).

We experimentally find an interesting phenomenon that some statistical indicators (e.g., mean and standard deviation) may significantly affect the model’s output, as shown in Fig. 2. Taking pre-trained AECRNet [45] as an example, by fine-tuning the mean and standard deviation (only a small perturbation) of deep features extracted by the encoder, the predicted image reconstructed via the decoder is able to manipulate the haze distribution.

Considering this, we propose an effective remedy, called Prompt-based Test-Time Dehazing (PTTD), which attempts to avoid training process and generate visually pleasing results during the inference phase. Specifically, we first apply a prompt generation module (PGM) to create a visual prompt image, which is later employed to obtain the appropriate values of the statistics. Similar to style transfer [24], the visual prompt accepts a haze-free image as input and inherits the haze distribution from the real hazy image via the operation of image-level normalization (ILN). Then, we employ a feature adaptation module (FAM) into the encoder of a pre-trained model (PTTD is a plug-and-play pipeline, and can take various dehazing models as its backbone) for adjusting the statistics. The adjusting values are calculated by taking prompt and real hazy input into consideration, and the adjustment is realized by the operation of feature-level normalization (FLN). Both of ILN and FLN are derived from adaIN [24], which is used to align statistics of the content with those of the style in feature space. We hope the dehazing results of the real hazy images can better fit human’s perception. To achieve this ultimate goal, the ILN is further revised to avoid color distortion and the FLN adapts features with some effective and mandatory restrictions. Fig. 3 shows the overall architecture of proposed PTTD.

As shown in Fig. 1, we apply the proposed PTTD

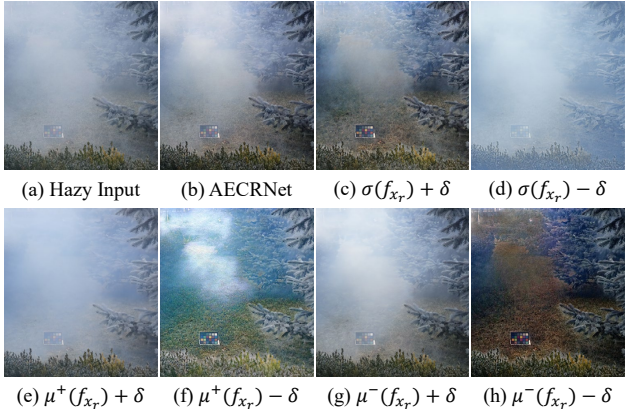


Figure 2. (a) is a real hazy input; (b) is the processing result of AECRNet [45], which is trained on synthetic data; (c)-(d) are the results by fine-tuning the standard deviation σ ; (e)-(h) are the results by fine-tuning the mean μ . In this experiment, the perturbation δ is set to a small constant, *i.e.*, $\delta = 0.01$.

to AECRNet [45] by slightly changing original structure (add PGM, FAM). We denote it as AECRNet-PTTD. The AECRNet-PTTD recovers clearer textures, more accurate color, less artifacts than the alternatives, demonstrating the superiority of proposed PTTD. Our main contributions can be summarized as follows:

- A novel dehazing pipeline called Prompt-based Test-Time Dehazing (PTTD) is proposed, which can adapt models pre-trained on synthetic data to real-world images during test-time. To the best of our knowledge, PTTD is first of a kind, where no training process (including training and test-time training) is demanded.
- PTTD aims to narrow the domain gap between synthetic and real by fine-tuning the statistics of encoding features extracted by models pre-trained on synthetic data. This is an innovative research direction.
- Further, we design a Prompt Generation Module (PGM) to obtain a visual prompt by image-level normalization (ILN). The prompt provides suitable perturbations for a Feature Adaptation Module (FAM) to adjust the statistics via feature-level normalization (FLN). PGM and FAM constitute our PTTD pipeline, which is flexible (model-agnostic) and outperforms SOTA methods in real image dehazing.

2. Related Work

2.1. Single Image Dehazing

Pioneers of image dehazing [6, 15, 16, 21, 44, 53] estimate the key components of ASM (*i.e.*, transmission map and atmospheric light) by leveraging handcraft priors induced from statistics of haze-free images, and then perform image dehazing. Although prior-based methods achieve im-

pressive dehazing performance, their effectiveness is constrained to hazy scenes which happen to satisfy the assumption they made.

With the rapid development of deep learning, learning-based methods have dominated the image dehazing domain. Early CNN-based methods [8, 28, 40, 51] utilize CNNs to estimate transmission map and atmospheric light. However, the inaccurate estimation of intermediate parameters will introduce the accumulated error. To avoid this, recent CNN-based and transformer-based methods [11, 13, 14, 19, 22, 23, 33, 38, 43, 45, 48, 52] discard the physical model and generate dehazing results or their residuals via the end-to-end paradigm. While learning-based methods demonstrate superior dehazing performance in synthetic domain, they usually suffer from performance degradation on real-world hazy scenes.

2.2. Real Image Dehazing

Recently, an increasing number of works have noticed the domain gap between synthetic domain and real domain, and tried to improve real-world dehazing performance. One category of these methods utilize real hazy images to reduce the domain gap [10, 17, 18, 26, 30–32, 41, 50]. DAD [41] employs CycleGAN for the translation between the synthetic domain and the real domain. PSD [10] fine-tunes pre-trained dehazing models on the real domain by establishing an unsupervised prior loss committee. However, due to the absence of paired data in real-world scenarios, complicate training strategies (*e.g.*, CycleGAN, prior loss) and their corresponding limitations are introduced. The other category aims to improve generalization performance of dehazing by exclusively utilizing synthetic images [42, 46, 47]. For example, Wu *et al.* [46] propose a new degradation pipeline to better align the synthetic domain with the real domain. Despite these efforts, without the aid of real hazy images, domain shift remains [46]. In order to avoid the inherent limitation of complicate training strategies and leverage the advantages of large-scale synthetic dataset, we propose a novel pipeline to perform feature adaptation on pre-trained models during only test-time.

3. Methodology

Let $D_S = \{x_s^i, y_s^i\}_{i=1}^{N_s}$ denote synthetic hazy-clean pairs and $D_R = \{x_r^i\}_{i=1}^{N_r}$ indicate a collection of real-world hazy images, where N_s and N_r denote the number of synthetic and real-world samples, respectively. A dehazing network \mathcal{N} trained on D_S often fails to generalize well to real data D_R , which can be attributed to the domain gap between D_S and D_R . Our PTTD aims to bridge the gap during the inference phase.

3.1. Motivation

Comparing a hazy image with a haze-free image, the difference is mainly observed in terms of luminance and contrast. We argue that these two image-level statistics are correlated closely with feature statistics, *i.e.*, mean μ and standard deviation σ . Adjusting the values of μ and σ in feature space can in turn affect the luminance and contrast of the reconstructed image, achieving haze removal effect. To validate this hypothesis, we firstly employ a dehazing model \mathcal{N} which is pre-trained on only synthetic hazy-clean pairs (without loss of generality, AECRNet [45] is adopted here) to perform dehazing on a real hazy input x_r . As shown in Fig. 2 (b), AECRNet achieves unsatisfactory dehazing result. Then, we apply a subtle perturbation δ on μ and σ of the extracted features through AECRNet’s encoder. Let f_{x_r} denotes the features, we adjust $\sigma(f_{x_r})$ to $\sigma(f_{x_r}) + \delta / \sigma(f_{x_r}) - \delta$ via a linear transformation. As shown in Fig. 2 (c) and (d), $\sigma(f_{x_r}) + \delta$ strengthens \mathcal{N} ’s dehazing effect, and $\sigma(f_{x_r}) - \delta$ makes the reverse optimization. Similar results can be observed in terms of $\mu(f_{x_r})$. Since the range of $\mu(f_{x_r})$ is $(-\infty, +\infty)$, we decompose it into $\mu^-(f_{x_r}) \in (-\infty, 0)$ and $\mu^+(f_{x_r}) \in [0, +\infty)$ for a more detailed investigation.

Motivated by this, we argue a possible solution which can narrow the domain gap is to adjust the statistics of f_{x_r} (with suitable perturbations) to make the features align with the synthetic domain. So the weight-fixed decoder of \mathcal{N} can reconstruct haze-free predictions.

3.2. Pipeline Overview

As illustrated in Fig. 3 (a), PTTD contains two major parts: pre-processing part and feature transformation part. In the pre-processing part, we employ a prompt generation module (PGM) to produce a visual prompt p , whose extracted features f_p are the target domain for guiding the adaption of f_{x_r} . As the key of our PTTD, feature transformation part can adopt most dehazing models as the backbone. In the feature transformation part, the feature adaption module (FAM) is employed into the encoder of \mathcal{N} to conduct the adaptation process for narrowing domain gap. We denote the new model with FAM as \mathcal{N}^\dagger . \mathcal{N}^\dagger takes x_r and p as inputs and outputs the reconstructed result \hat{J} .

3.3. Prompt Generation Module

Prompt generation module (PGM) is the key component of the pre-processing part. The goal of PGM is to generate a visual prompt p , which can guide the adjustment of statistics inside the FAM (offer appropriate values of mean μ and standard deviation σ). To fulfill this objective, the prompt p must meet two criteria: (1) it should be similar to the synthetic domain, so the encoder part of a certain pre-trained model can correctly extract the features. (2) it must has similar haze distribution with x_r , so the adaption could be

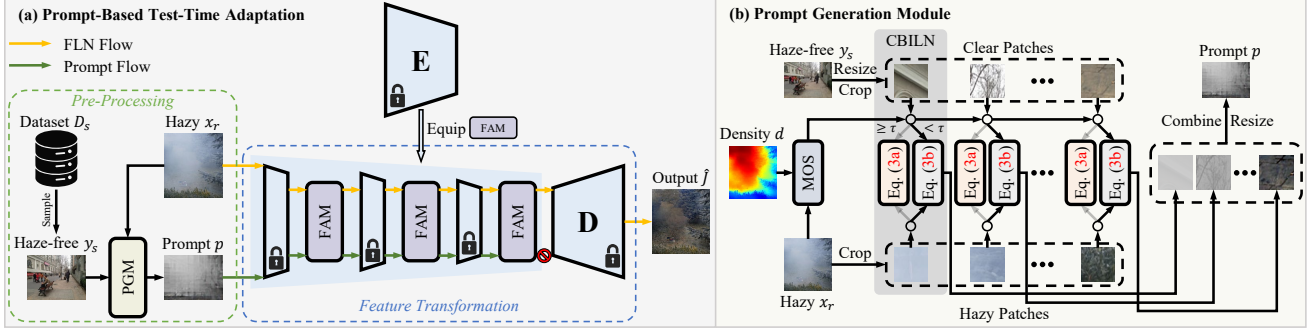


Figure 3. (a) The overall architecture of our Prompt-based Test-Time Dehazing (PTTD); (b) The proposed prompt generation module (PGM).

stable to avoid the collapse of the whole pipeline. These principles incline us to sample a haze-free image y_s from D_S , and then synthesize similar haze as x_r on y_s . For simplicity, the y_s is randomly chosen from the clean images of synthetic hazy-clean pairs.

Adaptive instance normalization (adaIN) [24] tries to enable arbitrary style transfer by aligning the channel-wise mean and variance of the content features with those of the style features. Accordingly, we adopt adaIN by taking x_r and y_s as the style input and content input, respectively. We denote it as image-level normalization (ILN) by aligning μ and σ of y_s with those of x_r :

$$p = \text{ILN}(y_s, x_r) = \sigma_c(x_r) \frac{y_s - \mu_c(y_s)}{\sigma_c(y_s)} + \mu_c(x_r), \quad (2)$$

where $\mu_c(\cdot) \in \mathbb{R}^C$ and $\sigma_c(\cdot) \in \mathbb{R}^C$ are mean and standard deviation, computed across the spatial dimensions for R,G,B channels.

As shown in Fig. 4 (c), simply adopting the adaIN scheme would fail to transfer the haze distribution from x_r to y_s , since light-haze and dense-haze regions may compromise each other and generate average results. We argue that μ and σ are global statistics, and the haze distribution (e.g., density) is inconsistent across the whole image. Therefore, we uniformly crop x_r and y_s into small patches without overlap¹ and apply ILN on patches. With this partition strategy, our ILN can effectively transfer the haze distribution from x_r to y_s . Fig. 4 (d) shows the generated prompt, sharing very similar haze with x_r .

The criterion (2) is definitely satisfied under this setting. We surprisingly find that criterion (1) is also met. We reveal that ILN with partition strategy can be viewed as the process of haze simulation based on ASM. By comparing Eq. (1) and Eq. (2), if the transmission map $t(x)$ is assumed to be a constant, both equations can be regarded as the linear transformation. With a sufficient number of partition

¹In practice, the resolutions of x_r and y_s may be different, we first resize y_s to the resolution of x_r to improve the flexibility.



Figure 4. (a) A real hazy image x_r ; (b) A haze-free image y_s from D_S ; (c) Prompt via direct ILN (adaIN); (d) Prompt via ILN with partition; (e) Prompt via CBILN with partition.

regions, the transmission map $t(x)$ of a certain patch can be approximately described as a fixed value, which satisfies the key assumption. In this situation, prompt generated via ILN with partition shares the same characteristics with the synthetic domain, since the prompt strictly follows the ASM.

Inspired by [31], we also take intra-domain gap (i.e., varicolored hazy scenes) into consideration to calibrate the color distortion. As illustrated in Fig. 4, the real hazy image is often varicolored (i.e., bluish here) and the generated prompt via ILN has similar color distribution. We argue that the prompt must be color balanced to avoid introducing color distortion in the predicted haze-free image. There have been many methods developed to provide color constancy, for example, the widely used gray world assumption [7, 39] hypothesizes that the average scene captured in an image is gray. We accordingly modify the ILN into color balanced ILN (CBILN) by replacing $\mu_c(x_r)$ and $\sigma_c(x_r)$ with corresponding mean values among R,G,B channels, i.e., $\bar{\mu} = \text{mean}(\mu_c(x_r))$ and $\bar{\sigma} = \text{mean}(\sigma_c(x_r))$.

$$p = \text{CBILN}(y_s, x_r) = \begin{cases} \text{ILN}(y_s, x_r), & \text{MOS}(x_r) \geq \tau \quad (3a) \\ \bar{\sigma} \frac{y_s - \mu_c(y_s)}{\sigma_c(y_s)} + \bar{\mu}, & \text{otherwise} \quad (3b) \end{cases}$$

Following [25], we utilize the measure of the spread of hue space (MOS) as our criteria to indicate whether a hazy region (which is determined by haze density d computed via DCP) is varicolored or not. Smaller MOS value means this image tends to be varicolored and CBILN should be

adopted, and vice versa. As illustrated in Fig. 3 (b), we utilize a threshold $\tau = 0.005$ for choosing Eq. (3a) or Eq. (3b) to generate the prompt.

3.4. Feature Adaptation Module

As stated before, our PTTD can be easily applied on dehazing models pre-trained on synthetic data. Typically, we adopt the encoder-decoder-like architecture which is quite prevalent among the pre-trained models [11, 13, 45]. In the feature transformation part, we keep the decoder part unchanged and modify the encoder part by inserting the feature adaptation module (FAM) after the basic blocks in every level (different spatial sizes indicate different levels). Taking the generated prompt p and a real hazy image x_r as inputs, the encoder part of a certain pre-trained dehazing model \mathcal{N} extracts corresponding features of different levels, denoted as f_p^l and $f_{x_r}^l$. We omit the level indicator for simplification, and one-level case is presented in this section. It is not laborious to extend to multiple levels. According to the key observation in Fig. 2, a naive idea is to align the channel-wise statistics of f_{x_r} with those of f_p (we denote this as feature-level normalization - FLN), meanwhile make sure the $\sigma_c(f_p)$ is larger than $\sigma_c(x_r)$ and the $\mu_c^+(f_p)/\mu_c^-(f_p)$ is smaller than $\mu_c^+(x_r)/\mu_c^-(x_r)$. However, since the visual prompt p is derived from a selected image, the values of $\sigma_c(f_p)$ and $\mu_c(f_p)$ may fluctuate. We need to add some restrictions on the statistical calculation of f_p , and the FLN can be formulated as:

$$\text{FLN}(f_{x_r}, f_p) = \sigma_c(f_p, f_{x_r}) \frac{f_{x_r} - \mu_c(f_{x_r})}{\sigma_c(f_{x_r})} + \mu_c(f_p, f_{x_r}), \quad (4)$$

where $\mu_c(f_p, f_{x_r})$ and $\sigma_c(f_p, f_{x_r})$ calculate the statistics of the target domain, providing appropriate perturbations for haze removal. The calculations are described by the pseudo code (see in Algorithm 1).

In step 2 to 5, the computed μ is less than or equal to $\mu_c(f_{x_r})$. The $\mu_c(f_p) \cdot \mu_c(f_{x_r}) \leq 0$ situation means these two items belong to different quadrants, and in this situation, we abort the feature adaptation from f_{x_r} to f_p to achieve more natural dehazing results.

In step 6 to 9, the computed σ is larger than or equal to $\sigma_c(f_{x_r})$. Although applying a positive perturbation $+\delta$ on σ can yield positive gains for hazy regions, it may be overly aggressive if there is a significant magnitude of difference between the $\sigma_c(f_p)$ and $\text{mean}(\sigma_c(f_{x_r}))$. The condition $\frac{\sigma_c(f_p) - \text{mean}(\sigma_c(f_{x_r}))}{\text{std}(\sigma_c(f_{x_r}))} < \alpha$ avoids significant fluctuation, restricting the distance from the mean of $\sigma_c(f_{x_r})$. In our implementation, the hyper-parameter α is set to 2.

Algorithm 1: Feature-level normalization - FLN

Input: f_p, f_{x_r}
Output: \hat{f}_{x_r} ; // $\hat{f}_{x_r} = \text{FLN}(f_{x_r}, f_p)$

- 1 compute $\mu_c(f_p), \mu_c(f_{x_r}), \sigma_c(f_p), \sigma_c(f_{x_r})$;
 /* **mean adaptation** */
- 2 **if** $\mu_c(f_p) \cdot \mu_c(f_{x_r}) > 0$ **then**
- 3 | $\mu_c(f_p, f_{x_r}) \leftarrow \min(\mu_c(f_p), \mu_c(f_{x_r}))$;
- 4 **else**
- 5 | $\mu_c(f_p, f_{x_r}) \leftarrow \mu_c(f_{x_r})$;
- 6 /* **std adaptation** */
- 6 **if** $\frac{\sigma_c(f_p) - \text{mean}(\sigma_c(f_{x_r}))}{\text{std}(\sigma_c(f_{x_r}))} < \alpha$ **then**
- 7 | $\sigma_c(f_p, f_{x_r}) \leftarrow \max(\sigma_c(f_p), \sigma_c(f_{x_r}))$;
- 8 **else**
- 9 | $\sigma_c(f_p, f_{x_r}) \leftarrow \sigma_c(f_{x_r})$;
- 10 $\hat{f}_{x_r} \leftarrow \sigma_c(f_p, f_{x_r}) \frac{f_{x_r} - \mu_c(f_{x_r})}{\sigma_c(f_{x_r})} + \mu_c(f_p, f_{x_r})$

4. Experiments

4.1. Experimental Configuration

Datasets. Our proposed PTTD pipeline is a test-time approach and model-agnostic, which can be regarded as a basic module to be plugged into most state-of-the-art dehazing models. Therefore, we don't need training data, and PTTD is free of training. Moreover, we adopt total six real-world datasets for evaluation. Four datasets with ground truths (O-HAZE [2], I-HAZE [1], NH-HAZE [4] and Dense-Haze [3]), and two datasets without ground truths (RTTS [29] and Fattal's [16]). O-HAZE, I-HAZE, NH-HAZE and Dense-Haze consist of 45, 35, 55 and 55 pairs of real hazy and corresponding haze-free images captured in various scenes. RTTS contains over 4000 real hazy images with diverse scenes, and haze-free images are not provided. In addition, Fattal's dataset with 31 classical real hazy images is also included for evaluation.

Implementation Details. We select three state-of-the-art models pre-trained on synthetic data as the backbone to comprehensively show the flexibility of our PTTD pipeline, including a CNN-based (*i.e.*, AEARNet [45]), a transformer-based (*i.e.*, Dehazformer [43]), and a general image restoration model (*i.e.*, NAFNet [9]). For fair comparisons, we re-train these three models on the same data built by Wu *et al.* [46]², and apply the proposed PTTD to narrow the domain gap from synthetic to real. The model with PTTD is denoted with suffix '-PTTD'. Typically, we traverse the haze-free images in Wu's dataset [46] (take it as y_s) and calculate the PSNR values (of AEARNet-PTTD model) on NH-HAZE2 [5] to search the top-performing y_s

²We find that the re-trained models on Wu's dataset [46] outperform the original models.

Method	O-HAZE		I-HAZE		NH-HAZE		Dense-Haze	
	PSNR \uparrow	SSIM \uparrow	PSNR \uparrow	SSIM \uparrow	PSNR \uparrow	SSIM \uparrow	PSNR \uparrow	SSIM \uparrow
(TIP'20) DeepDCP	16.92	0.6789	14.92	0.7171	13.04	0.4603	11.37	0.4505
(IJCV'21) YOLY	15.83	0.6640	15.21	0.6870	12.37	0.4561	11.60	0.4534
(CVPR'21) Zero-Restore	16.65	0.7536	16.56	0.7909	11.29	0.5151	12.29	0.4411
(CVPR'20) DAD	18.36	0.7484	18.02	0.7982	14.34	0.5564	13.51	0.4627
(CVPR'21) PSD	11.66	0.6831	13.79	0.7379	10.62	0.5246	9.74	0.4311
(CVPR'22) D4	16.96	0.7229	15.64	0.7294	12.67	0.5043	11.50	0.4500
(CVPR'23) RIDCP	16.52	0.7154	16.88	0.7794	12.32	0.5341	9.853	0.4525
(TIP'23) Dehazeformer	15.23	0.7437	17.42	0.8184	11.78	0.5423	9.25	0.4425
(Ours) Dehazeformer-PTTD	17.84 ^{+2.61}	0.7925 ^{+0.0488}	17.98 ^{+0.56}	0.8186 ^{+0.0002}	13.26 ^{+1.48}	0.5807 ^{+0.0384}	11.99 ^{+2.74}	0.4681 ^{+0.0256}
(ECCV'22) NAFNet	18.16	0.7783	17.03	0.8095	13.17	0.5367	10.45	0.4514
(Ours) NAFNet-PTTD	19.63 ^{+1.47}	0.8094 ^{+0.0311}	17.94 ^{+0.81}	0.8280 ^{+0.0185}	14.08 ^{+0.91}	0.5765 ^{+0.0398}	13.23 ^{+2.78}	0.4787 ^{+0.0273}
(CVPR'21) AECRNet	17.24	0.7640	16.72	0.8098	12.65	0.5326	8.59	0.4325
(Ours) AECRNet-PTTD	20.23 ^{+2.99}	0.8145 ^{+0.0505}	18.47 ^{+1.75}	0.8198 ^{+0.0100}	14.54 ^{+1.89}	0.5932 ^{+0.0606}	13.67 ^{+5.08}	0.4440 ^{+0.0115}

Table 1. Benchmark results of various dehazing methods on O-HAZE, I-HAZE, NH-HAZE, and Dense-Haze datasets. These four datasets contain the ground-truths for reference-based evaluation metrics’ calculations. **Bold** numbers indicate that the proposed PTTD profile can successfully help boost the performance.

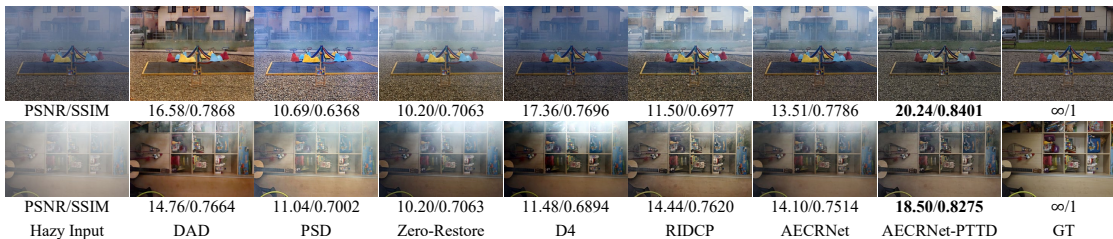


Figure 5. Dehazing results of various methods on O-HAZE. We choose AECRNet-PTTD to compare with SOTA dehazing methods. The PSNR/SSIM values are listed below the sub-images. Please zoom in on screen for a better view.

³. The chosen y_s is illustrated in Fig. 4 (b). In PGM, we cropped square patches from resized y_s by setting side length to $\frac{W}{10}$, where W denotes the width of the real hazy input x_r .

4.2. Experiments on datasets with labels

We first employ O-HAZE [2], I-HAZE [1], NH-HAZE [4] and Dense-Haze [3] datasets to evaluate our PTTD profile. With the labels (*i.e.*, haze-free images), reference-based metrics PSNR and SSIM are utilized to measure the performance. The quantitative comparisons on these four datasets are summarized in Tab. 1. We observe that by employing PTTD, robust improvements can be achieved on selected models, proving the effectiveness of this novel pipeline.

In addition, we also compare the models with ‘-PTTD’ suffix with some recent real image dehazing methods (DAD [41], PSD [10], D4 [47], and RIDCP [46]), an unsupervised method (DeepDCP [18]), and two zero-shot methods (YOLY [30], Zero-Restore [26]). AECRNet-PTTD achieves state-of-the-art performance on O-HAZE, I-HAZE and NH-HAZE. Specifically, compared with DAD [41], AECRNet-PTTD achieves 1.87 dB and 0.0661 gains in

³NH-HAZE2 dataset is adopted in the famous New Trends in Image Restoration and Enhancement (NTIRE) competition [5], and has no intersection with the testing datasets (including NH-HAZE).

terms of PSNR and SSIM on O-HAZE. Note that, the same y_s is utilized for all models and for all datasets. We don’t search the best-performing y_s for individual experiment. We believe better performance can be achieved by searching optimal y_s for each dataset.

We provide some qualitative comparisons of various methods on O-HAZE in Fig. 5. Note that, there is still a significant amount of haze, remaining in the predicted images of {PSD, Zero-Restore, D4, RIDCP, AECRNet}. DAD removes the haze successfully. However, the overall predictions tend to be warm-toned and some high-frequency information is also lost. Our proposed AECRNet-PTTD restores images with clearer details and less color distortion, which are closer to the ground-truths. More experimental results can be found in the supplementary materials.

4.3. Experiments on RTTS and Fattal’s

We then employ RTTS [29] and Fattal’s [16] datasets to evaluate our PTTD profile. Since there is no clean images in these two datasets, we embed some non-reference metrics (*e.g.*, FADE [12], BRISQUE [35], PAQ2PIQ [49], and MUSIQ [27]) for quantitative evaluation.

The quantitative results are presented in Tab. 2. We also take the real image dehazing methods {DAD, PSD, D4, RIDCP} into the comparison. With PTTD profile, the se-

Method	RTTS				Fattal's dataset			
	FADE↓	BRISQUE↓	PAQ2PIQ↑	MUSIQ↑	FADE↓	BRISQUE↓	PAQ2PIQ↑	MUSIQ↑
Hazy Input	2.576	37.01	66.05	53.77	1.061	21.08	71.54	63.25
(CVPR'20) DAD	1.131	32.93	66.79	49.88	0.4838	29.64	71.56	58.64
(CVPR'21) PSD	1.044	22.22	70.43	52.80	0.4161	23.61	76.02	63.04
(CVPR'22) D4	1.406	34.52	66.84	53.57	0.4109	20.33	73.13	63.27
(CVPR'23) RIDCP	0.9180	21.38	70.82	59.38	0.4083	20.05	74.64	66.88
(TIP'23) Dehazeformer	1.047	21.62	69.90	58.46	0.4399	21.70	74.72	67.15
(Ours) Dehazeformer-PTTD	0.7905 ^{-0.2565}	17.34 ^{-4.28}	71.45 ^{+1.55}	61.04 ^{+2.68}	0.4164 ^{-0.0235}	19.68 ^{-2.02}	75.70 ^{+0.98}	69.52 ^{+2.37}
(ECCV'22) NAFNet	1.121	26.25	70.08	58.89	0.4183	19.80	74.12	65.91
(Ours) NAFNet-PTTD	0.8267 ^{-0.2943}	22.72 ^{-3.53}	70.97 ^{+0.89}	59.79 ^{+0.90}	0.4289 ^{+0.0106}	18.75 ^{-1.05}	74.65 ^{+0.53}	66.98 ^{+1.07}
(CVPR'21) AECRNet	1.285	23.97	70.07	58.30	0.4319	21.44	74.41	66.83
(Ours) AECRNet-PTTD	0.7120 ^{-0.5740}	16.63 ^{-7.34}	72.04 ^{+1.97}	62.11 ^{+3.81}	0.3825 ^{-0.0494}	19.31 ^{-2.13}	75.01 ^{+0.60}	67.69 ^{+0.86}

Table 2. Quantitative comparisons of various dehazing methods on RTTS dataset and Fattal’s dataset. These two datasets lack ground-truths. Thus, non-reference metrics are employed to indicate the recovery quality. **Bold** numbers indicate the proposed PTTD profile can successfully boost the performance.

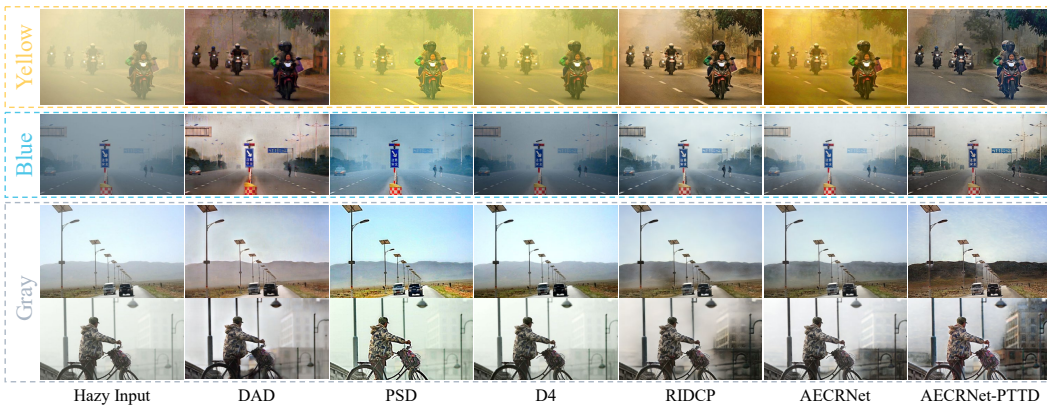


Figure 6. Dehazing results of various methods on RTTS. We choose AECRNet-PTTD to compare with SOTA dehazing methods. Please zoom in on screen for a better view.

lected models achieve robust performance improvements on RTTS. When it comes to Fattal’s dataset, only NAFNet-PTTD fails to boost the performance in terms of FADE. Note that, RTTS has relatively larger number of images than Fattal’s (4332 vs. 31). The metrics measured on latter tend to be unstable and biased. AECRNet-PTTD achieves state-of-the-art performance on RTTS dataset in terms of all non-reference metrics. Similarly, the same y_s is utilized for all models and for both datasets.

Fig. 6 shows the qualitative comparisons on RTTS. When it comes to varicolored scenes, all the comparative methods fail to eliminate color cast except DAD. However, DAD suffers from undesired artifacts, which is unacceptable. Only AECRNet-PTTD can restore the visibility and tackle the color balance simultaneously. More experimental results can be found in the supplementary materials.

4.4. Ablation Study

In this section, we perform ablation study to verify the effectiveness of (1) PGM, and (2) FAM. We utilize pre-trained AECRNet [45] as the backbone and measure the PSNR and

	PGM			FAM		Selected Prompt		Random Prompt	
	ILN	CBILN	partition	adaIN	FLN	PSNR↑	SSIM↑	PSNR↑	SSIM↑
	-	-	-	-	-	17.24	0.7643	-	-
①	-	-	-	✓	-	16.70	0.7638	14.58	0.7272
②	✓	-	-	✓	-	16.90	0.7777	13.92	0.7211
③	✓	-	✓	✓	-	18.28	0.7862	16.11	0.7501
④	-	✓	✓	✓	-	19.46	0.8068	17.81	0.7826
⑤	-	✓	✓	-	✓	20.23	0.8145	19.51	0.8008

Table 3. Ablation study of PGM and FAM on O-HAZE. The metrics in ‘Random Prompt’ are averaged on all involved y_s .

SSIM values on O-HAZE dataset. Since the performance of our PTTD correlates to the haze-free image y_s sampled from D_S , we divide ablation experiments into two groups: (1) selected prompt: elaborately search through the clean images in Wu’s dataset [46] and evaluate the performance on NH-HAZE2 dataset [5] to determine the top-performing y_s . The selected y_s is then utilized for all experiments. (2) random prompt: randomly select one clean image from Wu’s dataset [46] and the experimental results are averaged on all involved y_s .

Discussion on the selection of y_s . The selection of the

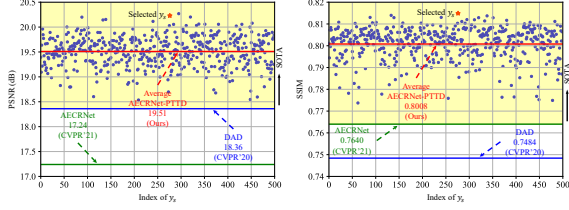


Figure 7. We randomly choose a clean image in Wu’s dataset [46] as y_s , and plot the performance scatter graph of each y_s on O-HAZE. Note that, AECRNet-PTTD model is adopted here.

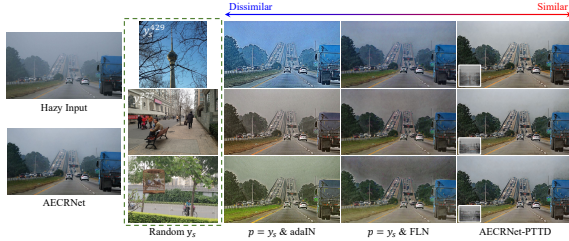


Figure 8. Visual results of a certain hazy input with varied y_s . The superscript of y_s^i denotes the index number of Wu’s [46] dataset.

haze-free image is technically unlimited. As shown in Tab. 3, though the model using the selected y_s performs better than that with random y_s , the latter still reaches state-of-the-art performance. As illustrated in Fig. 7, even the worst-performing y_s from the ‘Random Prompt’ achieves higher PSNR values than DAD and AECRNet. We also experimentally find that by choosing varied y_s , the final recovered results are very similar and indistinguishable (see in Fig. 8), though the intermediate results may be different. There is no doubt that the model with random y_s works relatively well, indicating the robustness of our proposed PTTD profile.

Effectiveness of PGM. The pre-trained AECRNet is regarded as the baseline (the first row of Tab. 3). PGM is designed to generate a visual prompt, and consists of image-level normalization (ILN), color balanced ILN (CBILN), and partition strategy. To analyze the role of each part, four variants are adopted: (1) PGM is not applied and $p = y_s$; (2) $p = \text{ILN}(y_s, x_r)$; (3) $p = \text{ILN}(y_s, x_r) + \text{partition strategy}$; (4) $p = \text{CBILN}(y_s, x_r) + \text{partition strategy}$. The experimental results are summarized in Tab. 3. Directly taking y_s as p or simply adopting ILN to generate p can not help the haze removal and may cause performance drop (16.90 dB and 16.70 dB). Partition strategy can guarantee the haze distribution of p to be consistent with x_r and similar to synthetic domain, boosting the performance of ILN to 18.28 dB. By taking the intra-domain gap into consideration, upgrading ILN to CBILN pushes the performance forward to 19.46 dB.

Effectiveness of FAM. The function of FAM is to adapt the

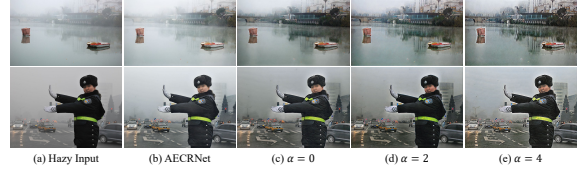


Figure 9. Ablation study of different values of α .

Method	YOLY	Zero-Restore	DAD	PSD	RIDCP	AECRNet	AECRNet-PTTD
#Param. (M)	39.99	0.25	54.59	33.11	28.72	2.611	2.611
Runtime (ms)	21852	533847	19.16	29.96	173.2	23.48	65.57

Table 4. Inference time comparisons of various dehazing methods. The results are measured on color images with 512×512 spatial resolution. The processing time of YOLY [30] and Zero-Restore [26] approaches is unacceptable, since they require time-consuming training procedures for every single input.

features f_{x_r} and make them match with the target domain (i.e., f_p). We freeze the design of PGM as CBILN with partition, and compare proposed FLN with adaIN. The main difference is based on the calculations of statistics of the target domain. The experimental results are summarized in the bottom two rows of Tab. 3. With more restrictions, FLN outperforms adaIN by 0.77 dB. In addition, we also conduct ablation study on the hyper-parameter α , and the qualitative results are illustrated in Fig. 9. The value of α and the haze removal effect are proportional to each other. Over-enhanced results may be produced when α is greater than 2, and we can obtain under-enhanced results if α is less than 2. We set α to 2 to balance the removal effect and visual perception.

Inference Time. The PTTD is promising to narrow the domain gap between the synthetic and real datasets, where no training process (including training and test-time training) is demanded. However, PTTD profile inevitably increases the inference time of the underlying backbone, due to the calculation procedures of PGM and FAM. Tab. 4 demonstrates the comparative results of various dehazing methods. It is worth mentioning that the increase in inference time of our AECRNet-PTTD against the backbone (i.e., AECRNet [45]) is not noticeable. In addition, another advantage is that our PTTD framework does not increase the parameter size.

5. Conclusion

In this paper, we propose a PTTD pipeline to adapt models pre-trained on synthetic data to real-world images during the inference phase. We reveal that fine-tuning the statistics (with suitable perturbations) of encoding features extracted by a certain pre-trained model can help narrow the domain gap between synthetic and real. Accordingly, a PGM is employed to generate a visual prompt by transferring the haze

distribution from the real hazy image to the haze-free image (via the operation of ILN), providing the perturbations for subsequent features adaptation. Then we modify the encoder of a pre-trained model by adding FAMs to adjust the statistics of extracted features (via the operation of FLN). Extensive experimental results clearly show the flexibility and superiority of our PTTD.

References

- [1] Cosmin Ancuti, Codruta O. Ancuti, Radu Timofte, and Christophe De Vleeschouwer. I-HAZE: A Dehazing Benchmark with Real Hazy and Haze-Free Indoor Images. In *CVPRW*, pages 620–631, 2018. 5, 6
- [2] Codruta O. Ancuti, Cosmin Ancuti, Radu Timofte, and Christophe De Vleeschouwer. O-haze: A dehazing benchmark with real hazy and haze-free outdoor images. In *Proceedings of the IEEE Conference on Computer Vision and Pattern Recognition (CVPR) Workshops*, 2018. 5, 6
- [3] Codruta O. Ancuti, Cosmin Ancuti, Mateu Sbert, and Radu Timofte. Dense-Haze: A Benchmark for Image Dehazing with Dense-Haze and Haze-Free Images. In *ICIP*, pages 1014–1018. IEEE, 2019. 5, 6
- [4] Codruta O. Ancuti, Cosmin Ancuti, and Radu Timofte. Nh-haze: An image dehazing benchmark with non-homogeneous hazy and haze-free images. In *Proceedings of the IEEE/CVF Conference on Computer Vision and Pattern Recognition (CVPR) Workshops*, 2020. 5, 6
- [5] Codruta O. Ancuti, Cosmin Ancuti, Florin-Alexandru Vasluiianu, and Radu Timofte. Ntire 2021 nonhomogeneous dehazing challenge report. In *Proceedings of the IEEE/CVF Conference on Computer Vision and Pattern Recognition*, pages 627–646, 2021. 5, 6, 7
- [6] Dana Berman, Tali Treibitz, and Shai Avidan. Non-local image dehazing. In *CVPR*, pages 1674–1682, 2016. 1, 2
- [7] Gershon Buchsbaum. A spatial processor model for object colour perception. *Journal of the Franklin institute*, 310(1): 1–26, 1980. 4
- [8] Bolun Cai, Xiangmin Xu, Kui Jia, Chunmei Qing, and Dacheng Tao. Dehazenet: An end-to-end system for single image haze removal. *IEEE Transactions on Image Processing*, 25(11):5187–5198, 2016. 1, 3
- [9] Liangyu Chen, Xiaojie Chu, Xiangyu Zhang, and Jian Sun. Simple baselines for image restoration. In *European Conference on Computer Vision*, pages 17–33. Springer, 2022. 5
- [10] Zeyuan Chen, Yangchao Wang, Yang Yang, and Dong Liu. Psd: Principled synthetic-to-real dehazing guided by physical priors. In *Proceedings of the IEEE/CVF Conference on Computer Vision and Pattern Recognition (CVPR)*, pages 7180–7189, 2021. 1, 2, 3, 6
- [11] Zixuan Chen, Zewei He, and Zhe-Ming Lu. Dea-net: Single image dehazing based on detail-enhanced convolution and content-guided attention. *arXiv preprint arXiv:2301.04805*, 2023. 2, 3, 5
- [12] Lark Kwon Choi, Jaehee You, and Alan Conrad Bovik. Referenceless prediction of perceptual fog density and perceptual image defogging. *IEEE Transactions on Image Processing*, 24(11):3888–3901, 2015. 6
- [13] Hang Dong, Jinshan Pan, Lei Xiang, Zhe Hu, Xinyi Zhang, Fei Wang, and Ming-Hsuan Yang. Multi-scale boosted dehazing network with dense feature fusion. In *Proceedings of the IEEE/CVF conference on computer vision and pattern recognition*, pages 2157–2167, 2020. 2, 3, 5
- [14] Jiangxin Dong and Jinshan Pan. Physics-based feature dehazing networks. In *European Conference on Computer Vision*, pages 188–204. Springer, 2020. 3
- [15] Raanan Fattal. Single image dehazing. *ACM transactions on graphics (TOG)*, 27(3):1–9, 2008. 2
- [16] Raanan Fattal. Dehazing using color-lines. *ACM transactions on graphics (TOG)*, 34(1):1–14, 2014. 2, 5, 6
- [17] Yosef Gandelsman, Assaf Shocher, and Michal Irani. "double-dip": Unsupervised image decomposition via coupled deep-image-priors. In *Proceedings of the IEEE/CVF Conference on Computer Vision and Pattern Recognition (CVPR)*, 2019. 3
- [18] Alona Golts, Daniel Freedman, and Michael Elad. Unsupervised single image dehazing using dark channel prior loss. *IEEE Transactions on Image Processing*, 29:2692–2701, 2020. 2, 3, 6
- [19] Chun-Le Guo, Qixin Yan, Saeed Anwar, Runmin Cong, Wenqi Ren, and Chongyi Li. Image dehazing transformer with transmission-aware 3d position embedding. In *Proceedings of the IEEE/CVF Conference on Computer Vision and Pattern Recognition*, pages 5812–5820, 2022. 3
- [20] Kaiming He, Jian Sun, and Xiaoou Tang. Single image haze removal using dark channel prior. In *CVPR*, pages 1956–1963, 2009. 1
- [21] Kaiming He, Jian Sun, and Xiaoou Tang. Single image haze removal using dark channel prior. *IEEE transactions on pattern analysis and machine intelligence*, 33(12):2341–2353, 2010. 1, 2
- [22] Zewei He, Zixuan Chen, Ziqian Lu, Xuecheng Sun, and Zhe-Ming Lu. Accurate and lightweight dehazing via multi-receptive-field non-local network and novel contrastive regularization. *arXiv preprint arXiv:2309.16494*, 2023. 3
- [23] Ming Hong, Jianzhuang Liu, Cuihua Li, and Yanyun Qu. Uncertainty-driven dehazing network. *Proceedings of the AAAI Conference on Artificial Intelligence*, 36(1):906–913, 2022. 2, 3
- [24] Xun Huang and Serge Belongie. Arbitrary style transfer in real-time with adaptive instance normalization. In *Proceedings of the IEEE International Conference on Computer Vision (ICCV)*, 2017. 2, 4
- [25] Sobhan Kanti Dhara, Mayukh Roy, Debashis Sen, and Prabir Kumar Biswas. Color cast dependent image dehazing via adaptive airlight refinement and non-linear color balancing. *IEEE Transactions on Circuits and Systems for Video Technology*, 31(5):2076–2081, 2021. 4
- [26] Aupendu Kar, Sobhan Kanti Dhara, Debashis Sen, and Prabir Kumar Biswas. Zero-shot single image restoration through controlled perturbation of koschmieder’s model. In *Proceedings of the IEEE/CVF Conference on Computer Vision and Pattern Recognition*, pages 16205–16215, 2021. 3, 6, 8

- [27] Junjie Ke, Qifei Wang, Yilin Wang, Peyman Milanfar, and Feng Yang. Musiq: Multi-scale image quality transformer. In *Proceedings of the IEEE/CVF International Conference on Computer Vision*, pages 5148–5157, 2021. 6
- [28] Boyi Li, Xiulian Peng, Zhangyang Wang, Jizheng Xu, and Dan Feng. Aod-net: All-in-one dehazing network. In *Proceedings of the IEEE international conference on computer vision*, pages 4770–4778, 2017. 1, 3
- [29] Boyi Li, Wenqi Ren, Dengpan Fu, Dacheng Tao, Dan Feng, Wenjun Zeng, and Zhangyang Wang. Benchmarking single-image dehazing and beyond. *IEEE Transactions on Image Processing*, 28(1):492–505, 2018. 5, 6
- [30] Boyun Li, Yuanbiao Gou, Shuhang Gu, Jerry Zitao Liu, Joey Tianyi Zhou, and Xi Peng. You only look yourself: Un-supervised and untrained single image dehazing neural network. *International Journal of Computer Vision*, 129:1754–1767, 2021. 3, 6, 8
- [31] Yi Li, Yi Chang, Yan Gao, Changfeng Yu, and Luxin Yan. Physically disentangled intra- and inter-domain adaptation for varicolored haze removal. In *Proceedings of the IEEE/CVF Conference on Computer Vision and Pattern Recognition (CVPR)*, pages 5841–5850, 2022. 4
- [32] Huan Liu, Zijun Wu, Liangyan Li, Sadaf Salehkalaibar, Jun Chen, and Keyan Wang. Towards Multi-domain Single Image Dehazing via Test-time Training. In *CVPR*, pages 5831–5840, 2022. 3
- [33] Xiaohong Liu, Yongrui Ma, Zhihao Shi, and Jun Chen. Grid-dehazenet: Attention-based multi-scale network for image dehazing. In *Proceedings of the IEEE/CVF international conference on computer vision*, pages 7314–7323, 2019. 3
- [34] Ye Liu, Lei Zhu, Shunda Pei, Huazhu Fu, Jing Qin, Qing Zhang, Liang Wan, and Wei Feng. From synthetic to real: Image dehazing collaborating with unlabeled real data. In *Proceedings of the 29th ACM International Conference on Multimedia*, pages 50–58, 2021.
- [35] Anish Mittal, Anush Krishna Moorthy, and Alan Conrad Bovik. No-reference image quality assessment in the spatial domain. *IEEE Transactions on image processing*, 21(12):4695–4708, 2012. 6
- [36] Srinivasa G Narasimhan and Shree K Nayar. Vision and the atmosphere. *International journal of computer vision*, 48:233–254, 2002. 1
- [37] S. G. Narasimhan and S. K. Nayar. Contrast restoration of weather degraded images. *IEEE Transactions on Pattern Analysis and Machine Intelligence*, 25(6):713–724, 2003. 1
- [38] Xu Qin, Zhilin Wang, Yuanchao Bai, Xiaodong Xie, and Huizhu Jia. Ffa-net: Feature fusion attention network for single image dehazing. In *Proceedings of the AAAI Conference on Artificial Intelligence*, pages 11908–11915, 2020. 2, 3
- [39] Erik Reinhard, Michael Adhikhmin, Bruce Gooch, and Peter Shirley. Color transfer between images. *IEEE Computer graphics and applications*, 21(5):34–41, 2001. 4
- [40] Wenqi Ren, Si Liu, Hua Zhang, Jinshan Pan, Xiaochun Cao, and Ming-Hsuan Yang. Single image dehazing via multi-scale convolutional neural networks. In *European conference on computer vision*, pages 154–169. Springer, 2016. 1, 3
- [41] Yuanjie Shao, Lerenhan Li, Wenqi Ren, Changxin Gao, and Nong Sang. Domain adaptation for image dehazing. In *Proceedings of the IEEE/CVF Conference on Computer Vision and Pattern Recognition (CVPR)*, 2020. 1, 2, 3, 6
- [42] Pranjay Shyam, Kuk-Jin Yoon, and Kyung-Soo Kim. Towards domain invariant single image dehazing. In *Proceedings of the AAAI Conference on Artificial Intelligence*, pages 9657–9665, 2021. 3
- [43] Yuda Song, Zhuqing He, Hui Qian, and Xin Du. Vision transformers for single image dehazing. *IEEE Transactions on Image Processing*, 32:1927–1941, 2023. 3, 5
- [44] Robby T Tan. Visibility in bad weather from a single image. In *2008 IEEE conference on computer vision and pattern recognition*, pages 1–8. IEEE, 2008. 1, 2
- [45] Haiyan Wu, Yanyun Qu, Shaohui Lin, Jian Zhou, Ruizhi Qiao, Zhizhong Zhang, Yuan Xie, and Lizhuang Ma. Contrastive learning for compact single image dehazing. In *Proceedings of the IEEE/CVF Conference on Computer Vision and Pattern Recognition*, pages 10551–10560, 2021. 1, 2, 3, 5, 7, 8
- [46] Rui-Qi Wu, Zheng-Peng Duan, Chun-Le Guo, Zhi Chai, and Chongyi Li. Ridcp: Revitalizing real image dehazing via high-quality codebook priors. In *Proceedings of the IEEE/CVF Conference on Computer Vision and Pattern Recognition*, pages 22282–22291, 2023. 3, 5, 6, 7, 8
- [47] Yang Yang, Chaoyue Wang, Risheng Liu, Lin Zhang, Xiaojie Guo, and Dacheng Tao. Self-augmented unpaired image dehazing via density and depth decomposition. In *Proceedings of the IEEE/CVF conference on computer vision and pattern recognition*, pages 2037–2046, 2022. 2, 3, 6
- [48] Tian Ye, Mingchao Jiang, Yunchen Zhang, Liang Chen, Erkang Chen, Pen Chen, and Zhiyong Lu. Perceiving and modeling density is all you need for image dehazing. In *European Conference on Computer Vision*, pages 130–145, 2022. 3
- [49] Zhenqiang Ying, Haoran Niu, Praful Gupta, Dhruv Mahajan, Deepti Ghadiyaram, and Alan Bovik. From patches to pictures (paq-2-piq): Mapping the perceptual space of picture quality. In *Proceedings of the IEEE/CVF Conference on Computer Vision and Pattern Recognition*, pages 3575–3585, 2020. 6
- [50] Hu Yu, Jie Huang, Yajing Liu, Qi Zhu, Man Zhou, and Feng Zhao. Source-free domain adaptation for real-world image dehazing. In *Proceedings of the 30th ACM International Conference on Multimedia*, pages 6645–6654, 2022. 3
- [51] He Zhang and Vishal M Patel. Densely connected pyramid dehazing network. In *Proceedings of the IEEE conference on computer vision and pattern recognition*, pages 3194–3203, 2018. 3
- [52] Yu Zheng, Jiahui Zhan, Shengfeng He, Junyu Dong, and Yong Du. Curricular contrastive regularization for physics-aware single image dehazing. In *Proceedings of the IEEE/CVF Conference on Computer Vision and Pattern Recognition (CVPR)*, pages 5785–5794, 2023. 2, 3
- [53] Qingsong Zhu, Jiaming Mai, and Ling Shao. A fast single image haze removal algorithm using color attenuation prior. *IEEE transactions on image processing*, 24(11):3522–3533, 2015. 1, 2